J Mol Model (2003) 9:248–258
DOI 10.1007/s00894-003-0138-9

ORIGINAL PAPER

Roman Wrzalik · Katarzyna Merkel · Antoni Kocot

Ab initio study of phenyl benzoate: structure, conformational analysis, dipole moment, IR and Raman vibrational spectra

Received: 6 February 2003 / Accepted: 15 April 2003 / Published online: 11 July 2003

Abstract The molecular structure (bond distances and angles), conformational properties, dipole moment and vibrational spectroscopic data (vibrational frequencies, IR and Raman intensities) of phenyl benzoate were calculated using Hartree–Fock (HF), density functional (DFT), and second order Møller–Plesset perturbation theory (MP2) with basis sets ranging from 6-31G* to 6-311++G**. The theoretical results are discussed mainly in terms of comparisons with available experimental data. For geometric data, good agreement between theory and experiment is obtained for the MP2, B3LYP and B3PW91 levels with basis sets including diffuse functions. The B3LYP/6-31+G* theory level estimates the shape of the experimental functions for phenyl torsion around the Ph–O and Ph–C bonds well, but reproduces the height of the rotational barriers poorly. The B3LYP/6-31+G* harmonic force constants were scaled by applying the scaled quantum mechanical force field (SQM) technique. The calculated vibrational spectra were interpreted and band assignments were reported. They are in excellent agreement with experimental IR and Raman spectra.

Keywords Ab initio and density functional theory · Internal rotation · IR and Raman spectra · Vibrational assignments · Dipole moment

Introduction

The ester group (–C(=O)–O–) is the most frequently used molecular segment in designing ferroelectric and antiferroelectric liquid crystals (FLC and AFLC). Commonly, molecules consist of two or three such functional groups between phenyl rings or between a phenyl and the chiral chain of a molecule. The dipole moment of the group, which is reasonably high (1.8 D), [1] becomes the main contribution to the total dipole moment and results in spontaneous polarization in the ferroelectric phase. Nevertheless, conformational changes may vary the total dipole moment significantly (even by a few debyes). It is quite possible that the phase structure and resulting spontaneous polarization depend not only on the position of the ester groups but also on the conformations of the molecular segments. [2]

It is therefore important for designing the molecular structure, to determine the conformation of the core part and the chiral chain of FLC or AFLC molecules. The main part of the AFLC molecules frequently contains segments of the structure of phenyl benzoate (PB). Therefore, we have attempted to perform ab initio calculations in order to determine the structure of the PB molecule and to compare the results with experimental data.

The structure of phenyl benzoate in the crystalline phase was determined by X-ray diffraction, [3, 4] and that in the gas phase by gas electron diffraction (GED). [5] The analysis of the GED data was performed with the assumptions supported by ab initio RHF/6-31G** calculations. Adam and co-workers [6] have reported ab initio pseudopotential calculations for the periodic system. Some conclusions about the dihedral angle describing the phenyl ring (Ph) rotation around the O–Ph bond, were derived from the molar Kerr constant measurement, [7] the IR spectra [8] and analysis of the ^{1}H NMR spectra. [9]

Experimental

Phenyl benzoate (99% purity, melting point 245 K, boiling point 572 K) used for the vibrational spectroscopy measurements was purchased from the Sigma Chemical Co. The infrared (IR) absorption spectra from solid state samples were obtained by the KBr pellet technique and those from CCl_4 solution (0.01 M) using a cell with a 1-mm path length between potassium bromide windows. The spectra were measured at room temperature. The IR vapor spectra were recorded using a 10-cm path length cell with sodium chloride windows. The cell was

R. Wrzalik (✉) · K. Merkel · A. Kocot
Institute of Physics, University of Silesia,
Uniwersytecka 4, 40-007, Katowice, Poland
e-mail: wrzalik@us.edu.pl

electrically heated to 520 K and the vapor was kept in equilibrium with the liquid.

All IR measurements were performed using a commercial Fourier transform spectrometer, Bio-Rad FTS6000, equipped with a KBr beam splitter, a standard source and a DTGS Peltier-cooled detector. The spectra were recorded in the range 360–4,000 cm^{-1} at a spectral resolution of 1 cm^{-1} and the Norton–Berr apodization function was applied. Generally, 64 scans were accumulated to improve the quality of the spectra.

Raman spectra were recorded using a LabRam multichannel spectrometer comprising an Olympus BX40 confocal microscope. The spectrometer is equipped with a CCD detection system having 1,024 pixels along the dispersion axis and a grating with a groove density of 1,800 grooves mm^{-1}. The spectra were collected in the range 50–3,600 cm^{-1} at a spectral resolution of 2.8 cm^{-1} and with a data sampling interval 1 cm^{-1}. An air-cooled argon laser operating at 514.5 nm (JDS Uniphase) with approximately 30 mW of radiation power at the sample was used for excitation. A notch filter was set in the optical path to enhance the rejection of the exciting radiation (this limits the spectrum to Raman shifts over 50 cm^{-1}). Generally, the spectra were recorded ten times with an accumulation time of 60 s. The spectral frequencies were calibrated with the Si line and are believed to be accurate to ±1 cm^{-1}. The measurements of the crystalline phase were made at room temperature and for the liquid state at 345 K using a LINKAM THMS600 heating stage.

The absorption peak position was determined by the curvefit procedure using the Grams/AI software.

Calculation

Ab initio calculations were performed with the Gaussian98W program. [10] The geometry optimizations were carried out at the restricted Hartree–Fock (RHF) [11] and second order Møller–Plesset perturbation theory levels (MP2) [12] and with density functional theory (DFT). [13, 14, 15] Two types of functional were considered in the DFT calculation: Becke's hybrid three-parameter (exchange and correlated) functional [16] with the Lee–Yang–Parr correlation functional (B3LYP) [17, 18, 19] and Becke's hybrid three-parameter functional with the Perdew–Wang 1991 gradient-corrected correlation functional (B3-PW91). [20, 21] Standard Gaussian polarized and split-valence basis sets [11] were used: 6-31G** for RHF, 6-31G* and 6-31+G* for MP2 and 6-31G*, 6-31G**, 6-31+G*, 6-31+G**, 6-31++G*, 6-31++G** and 6-311++G** for the DFT methods.

The energy barriers for the internal rotation of the benzene rings around the O_3–C_4 and C_2–C_{10} bonds (torsion angles φ_1 and φ_2 respectively, see Fig. 1) were determined for the B3LYP/6-31G* and B3-LYP/6-31+G* levels. The approximate potential energy functions were calculated at intervals of 10°. In the calculations, the torsional angles, φ_1 or φ_2, were fixed at arbitrary selected values while the other geometrical parameters were optimized; relaxed potential energy scans were performed.

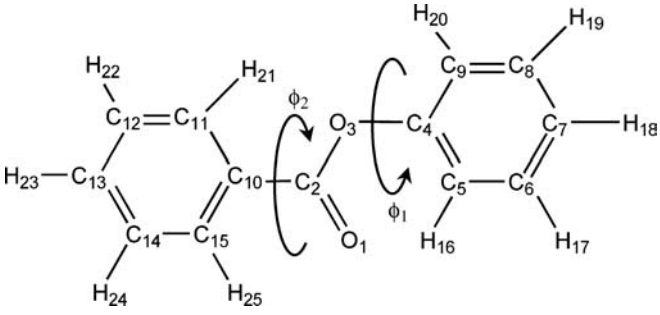

Fig. 1 Molecular structure with atom numbering of phenyl benzoate. φ_1 and φ_2 denotes the dihedral angles $C_2O_3C_4C_5$ and $O_3C_2C_{10}C_{11}$, respectively

IR and Raman spectra were computed using the harmonic approximation at the B3LYP/6-31G* and B3LYP/6-31+G* levels. All DFT optimization were carried out with the following convergence criteria used with Berny algorithm (all values in atomic units): the maximum component of the force was set to 0.00045, the root-mean square (RMS) of the forces calculated for the next step—smaller then 0.0003—the computed displacement for the next step—smaller than 0.0018—and the RMS of the displacement below 0.0012. These criteria restrict the dependence of the final geometry parameters on the initial starting geometry. For B3LYP frequency calculations, a pruned 99,590 grid was used to obtain a more accurate numerical integration; it is important for computing low frequency modes. Maximal force (in atomic units) that was lower than 3.6×10^{-5} after geometry optimization. The rotational frequencies were very close to zero, the translational frequencies smaller than 7.5 cm^{-1} and 11.4 cm^{-1}, respectively.

The theoretical vibrational frequencies, IR intensities and Raman activities were recalculated using Pulay's scaled quantum mechanical force field (SQM) methodology. [22, 23, 24] The SQM force field gives very good reproduction of the fundamental frequencies and is considered to approach the best accuracy that can be achieved in a harmonic treatment. This method also allows the assignment of the fundamental frequencies in molecules with a large number of atoms. [25, 26]

The experimental IR frequencies, mainly from the vapor phase and some from CCl_4 liquid solution, were used for the calculation. First, the DFT Cartesian force-constant matrix was transferred into nonredundant natural internal coordinates. Next, the scaling of the force field was performed in three steps. At the beginning, to get an initial description of fundamental frequencies and to compare them with the observed IR and Raman frequencies, the scaling factors proposed by Pulay and coworkers [24] were used. Then, a set of starting scaling factors was approximated from the ratio between the experimental and theoretical frequencies. Finally, the force field scaling factors for stretching vibrations of the

Table 1 Structural parameters of the phenyl benzoate molecule computed at the HF, B3LYP, MP2 theory levels and experimental

	Bonds (Å)						Bond angles (°)			Dihedral angles (°)	
	C=O	C*–O	C–O	C*–C	<CC>	<CH>	O=C*–O	C*–O–C	O–C*–C	φ_1	φ_2
X-ray	1.195	1.351	1.415	1.481	1.376	0.980	123.0	118.1	125.4	67.6	−8.7
GED	1.208	1.362	1.405	1.478	1.396	1.096	124.2	121.4	127.3	64.0	0.0
HF											
6-31G**	1.186	1.339	1.383	1.489	1.385	1.075	123.3	119.3	124.4	91.7	0.0
B3LYP											
6-31G*	1.211	1.370	1.396	1.489	1.396	1.086	124.0	121.0	124.7	49.5	1.2
6-31G**	1.211	1.370	1.396	1.489	1.396	1.085	124.0	121.2	124.7	47.8	1.2
6-31+G*	1.212	1.371	1.400	1.490	1.398	1.086	123.4	119.5	124.9	64.2	1.9
6-31+G**	1.212	1.371	1.400	1.490	1.397	1.085	123.5	119.5	124.9	64.2	1.9
6-31+G**	1.212	1.371	1.400	1.490	1.398	1.086	123.4	119.5	124.9	64.1	1.8
6-31++G**	1.212	1.371	1.400	1.490	1.397	1.085	123.5	119.5	124.9	64.0	1.8
6-311++G**	1.204	1.370	1.399	1.489	1.394	1.083	123.5	119.5	125.0	65.0	1.8
B3PW91											
6-31G*	1.209	1.365	1.390	1.486	1.394	1.086	124.0	120.5	124.7	51.1	1.7
6-31G**	1.209	1.365	1.390	1.486	1.394	1.085	124.1	120.7	124.7	49.3	1.6
6-31+G*	1.210	1.365	1.393	1.487	1.395	1.087	123.6	119.3	124.8	62.6	2.1
6-31+G**	1.210	1.365	1.393	1.487	1.395	1.086	123.6	119.3	124.8	62.5	2.1
6-31+G**	1.210	1.365	1.393	1.487	1.395	1.087	123.6	119.3	124.8	62.9	2.0
6-31++G**	1.210	1.365	1.393	1.487	1.395	1.086	123.6	119.4	124.8	62.3	2.1
6-311++G**	1.202	1.364	1.392	1.486	1.392	1.084	123.6	119.2	124.9	63.9	2.0
MP2											
6-31G*	1.217	1.376	1.403	1.486	1.396	1.087	123.8	116.7	125.1	64.2	1.1
6-31+G*	1.220	1.377	1.406	1.486	1.398	1.087	123.5	116.0	125.2	71.0	3.7

ester group were adjusted by minimizing the difference between the calculated and observed frequencies.

Geometrical structure

The atom numbering of phenyl benzoate is shown in the Fig. 1. In order to distinguish between the different types of bonds, we use the following shortcut notation: CH and CC for bonds of the phenyl ring, O–C and C–C* for phenyl-ester O_3–C_4 and C_{10}–C_2 bonds, respectively, and C*–O and C=O for C_2–O_3 and C_2–O_1 ester bonds, respectively.

Experimental (determined by X-ray diffraction and GED measurement) and calculated bond distances of phenyl benzoate are listed in Table 1 (for aromatic CC and CH bonds, only mean values are displayed and denoted as <CC>and <CH>, respectively).

The CH bond distances calculated at all levels give values very close to the experimental GED data and about 0.1 Å longer than those determined by the X-ray diffraction. It is well known that the uncertainties in crystallographic determinations of the H atom position are reasonably large and the CH bond lengths are usually 0.1–0.2 Å below the values for the gas phase. The aromatic CC bond distances from calculations are also closer to the GED geometric parameters. The B3LYP and B3PW91 data show only minor differences for all basis sets except for CC bond distances obtained with the 6-31++G** basis set, which differ slightly. The MP2 calculation also results in CC bond lengths very close to the gas-phase parameters while the RHF/6-31G* theory level gives much shorter values, closer to the crystal data.

The calculated and experimental carboxyl group O=C*–O, O=C*–C and C*–O–C bond angles are shown in the Table 1 (O_1–C_2–O_3, O_1–C_2–C_{10} and C_2–O_3–C_4 bond angles, respectively). The smallest difference between the experimental and calculated parameters is observed for the O=C*–O bond angle; the difference is below 1°. For the O=C*–C bond angle, the calculated values at all theory levels are quite close to the X-ray diffraction data and about 3° below the GED experimental value. All calculated O=C*–C bond angles are focused at 125° and depend weakly on the basis set. The C*–O–C band angle values are more scattered and lay between the GED and X-ray data. Only the MP2 level gives a value smaller than that determined by the X-ray measurement (about 2° smaller).

The most important finding for the structure of the core of mesogenic molecules formed by phenyl benzoate are the dihedral angles between the plane of the phenyl rings and the ester group (angles around the O–Ph and C*–Ph bonds). These angles are defined as $C_2O_3C_4C_5$ and $O_3C_2C_{10}C_{11}$ and are denoted by φ_1 and φ_2, respectively (see the Fig. 1).

In the crystal, the dihedral angles φ_1 and φ_2 are 67.5(2)° and 9.9(2)°, [4] respectively; the latter angle is probably affected by the crystal packing. The φ_1 gas-phase value, determined by the GED measurement is 64° (+26°, −12°). [5] The φ_2 dihedral angle in the gas phase is expected to be very close to 0° because of the strong conjugation between the carbonyl and phenyl group. The

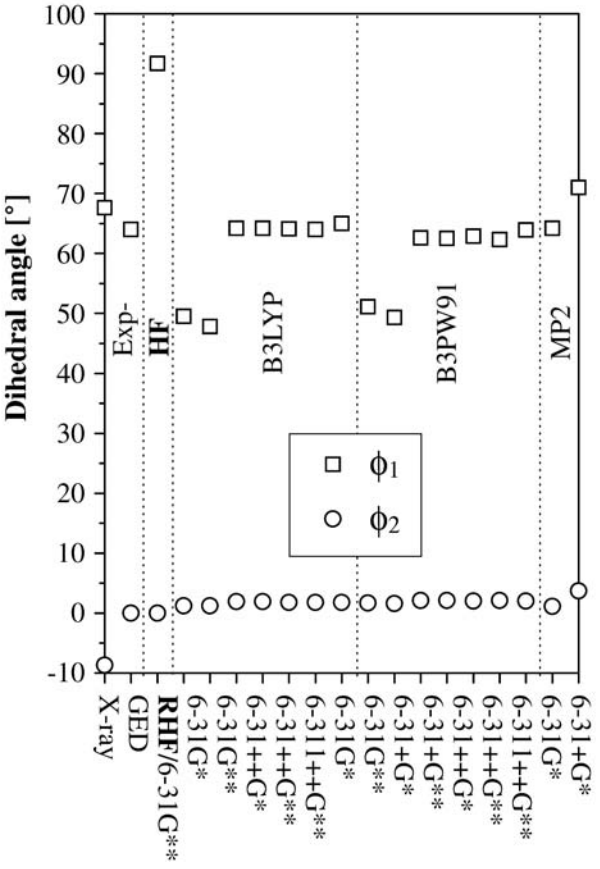

Fig. 2 Calculated and experimental dihedral angles φ_1 ($C_2O_3C_4C_5$) and φ_2 ($O_3C_2C_{10}C_{11}$) of phenyl benzoate

calculated values of the φ_1 and φ_2 angles are shown in Fig. 2 and are listed in the Table 1.

The RHF/6-31G** calculations give φ_1=91.7° and φ_2=0°, which lead to an almost perpendicular orientation of the phenyl rings with respect to each other. The B3LYP, B3PW91 and MP2 theory levels give good agreement between the calculated and experimental values. For the DFT methods, we observe excellent agreement of the φ_1 calculated values with the experimental ones for basis sets included diffusion functions. The 6-31G* and 6-31G** basis sets give much worse predictions of the φ_1 angle. The calculated φ_2 dihedral angle values, for all theory levels, are close to 0°, as expected (the values lie in the range 0–4°).

In the case of semiempirical methods, AM1 predicts a very realistic value of the dihedral angles: φ_1=50.3°, φ_2=3.2°. The PM3 calculation give the values φ_1=87.3° and φ_2=40.4°, very far from the experimental results.

We have also compared the calculated and the experimental GED structures of the phenyl benzoate molecule by superimposing the theoretical and experimental models and minimizing the distances between atoms (structures were frozen and molecules were rotated and translated to get the smallest RMS distances between atoms). The RMS distances for all models are listed in the Table 2. For the DFT (B3LYP and B3PW91) and MP2 theory levels the smallest values of the RMS distance were obtained for the basis set included diffuse functions. The orbitals with diffuse functions occupy a larger region of space and make the φ_1 dihedral angle larger. This reflects the important influence of electron lone pairs on the molecular structure (especially on the dihedral angles).

Table 2 The distance RMS (in Å) for the HF, B3LYP, B3PW91 and MP2 theory levels

	B3LYP	B3PW91	MP2	HF
6-31G*	0.0370	0.0328	0.3466	–
6-31G**	0.0404	0.0360	–	0.3445
6-31+G*	0.0308	0.0286	0.0283	–
6-31+G**	0.0307	0.0284	–	–
6-31++G*	0.0304	0.0287	–	–
6-31++G**	0.0303	0.0280	–	–
6-311++G**	0.0310	0.0292	–	–

Barriers to internal rotations

The phenyl benzoate molecule has three degrees of freedom for internal rotation, around the bonds C*–O (C_2–O_3), O–C (O_3–C_4) (which changes the dihedral angle φ_1) and C–C* (C_{10}–C_2) (described by the dihedral angle φ_2). It is well known from the literature that torsion around the C*–O bond is fairly rigid. [5, 27, 28] The molecular mechanics (MM) method gave approximate values of the rotational barriers: [8] 5.2, 0.95 and 1.16 kcal mol^{-1} for the rotation about C*–O, O–C and C–C* bonds, respectively. Sun [29] has estimated the O(ester)–C(carbonyl) energy barrier as more than 12 kcal mol^{-1}. This means that the C*–O rotation barrier is much higher than those for O–C and C–C*. For this reason, the conformational stability of phenyl benzoate was determined by examining the internal rotations of phenyl ring rotors around the O–C and C–C* bonds only. The potential energy functions of φ_1 and φ_2 were calculated at the B3LYP/6-31G* and B3LYP/6-31+G* levels. The calculation was performed at intervals of 10° for the dihedral angles, φ_1 or φ_2, which were fixed at arbitrarily selected values while the other geometrical parameters were optimized. The resulting potential curve was described by the function: [30, 31]

$$V(\phi) = V_2/2[1 - \cos(2\phi)] + V_4/2[1 - \cos(4\phi)]$$

The calculated potential functions are shown in Fig. 3 and their potential parameters are listed in Table 3. The values of the rotational barriers ΔV were calculated as an energy difference between the minimum and maximum values of the function $V(\varphi)$.

The B3LYP/6-31+G* scan gives much better prediction of the potential function, particularly for rotation around the O–C bond. We observe two maxima: the higher at φ_1=0° with the barrier height ΔV=0.72 kcal mol^{-1} and a much smaller one at φ_1=90° with ΔV=0.07 kcal mol^{-1}. The first rotational barrier at φ_1=0°

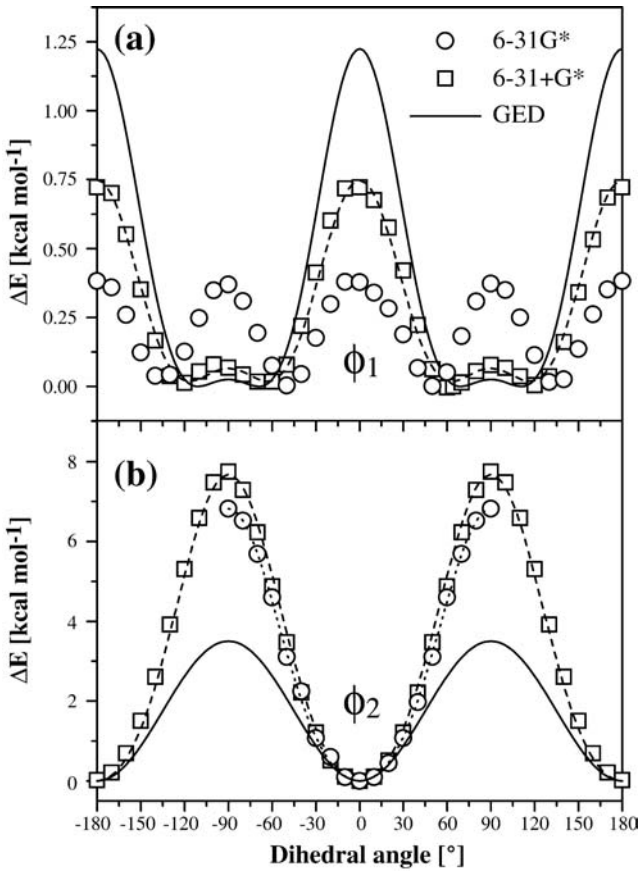

Fig. 3a–b Calculated and experimental (GED) potential energy functions for torsional motion of phenyl benzoate relative to the minimum value. **a** The potential function for torsion about the O_3–C_4 bond. **b** The potential function for torsion about the C_2–C_{10} bond

Table 3 Potential function parameters (in kcal mol^{-1}) for rotation around the O_3–C_4 (dihedral angle φ_1) and C_2–C_{10} bonds (dihedral angle φ_2): rotational barrier ΔV, function parameters V_2 and V_4

kcal mol^{-1}	φ_1	φ_2
B3LYP/6-31G*		
ΔV	0.38 at 0° and 90°	7.5 at 90°
B3LYP/6-31+G*		
ΔV	0.72 at 0° 0.07 at 90°	6.8 at 90°
V_2	–0.68	6.8
V_4	–0.29	–0.81
Experimental GED		
ΔV	1.2 at 0° 0.03 at 90°	3.5
V_2	–1.0	3.5
V_4	0.0	–

is almost two times smaller than the experimental one (ΔV=1.2 kcal mol^{-1}) but the shape of the potential curve is predicted well. In comparison, the calculation at the B3LYP/6-31G* level also shows two maxima at φ_1=0° and 90° but with the same height of the rotational barrier ΔV=0.38 kcal mol^{-1}.

The rotational barrier and the potential minimum for the O–C torsion are determined by the steric repulsion between the phenyl ring and the oxygen atom in the carboxyl group and the conjugation between the ester group and the phenyl ring. Conjugation favors the parallel arrangement of the C=O bond and the phenyl ring because the repulsion forces act in the opposite direction. The position of the potential minimum (64.2°) and the barrier height (0.71 kcal mol^{-1}) are consequences of the balance between these interactions.

For the φ_2 torsion, the calculated potential functions are very similar at the B3LYP/6-31G* and B3LYP/6-31+G* levels. The strong rotational barrier at 90° has values ΔV=7.5 and 6.8 kcal mol^{-1}, respectively, and they are about two times higher than the experimental result ΔV=3.5 kcal mol^{-1}. The barrier height obtained with the basis set with diffuse functions is closer to the value determined by the GED experiment. Our results correspond well with Meier and Kogliṅs prediction for benzaldehyde. [32] They concluded that the DFT methods strongly overestimate the rotational barrier around the C(phenyl)–C(aryl) bond and have suggested that molecules comprising a phenyl ring with a π-conjugated substituent cause problems with respect to the rotational energy potential calculation. The relatively big difference between the experimental and theoretical heights of the rotational barriers can be attributed to the fact that DFT methods do not involve dispersion interactions. [33, 34]

To take into consideration the dispersion interaction, MP2/6-31+G* calculation for the dihedrals of the maximum and minimum of the potential function were performed (the φ_1 angle was fixed at arbitrarily selected values while the other geometrical parameters were optimized). The energy difference for the geometry with φ_1=71° (the minimum) and φ_1=0° (the maximum) was 2.9 kcal mol^{-1}, more than two times higher than the experimental rotational barrier. The van der Waals interactions are probably overestimated.

Dipole moment

The dipole moment of the PB molecule was computed at the different theory levels employed in this work. It lies nearly parallel to the C=O bond and slightly out of the ester-group plane. The values of the dipole moment μ, the angle α between the dipole and the C=O bond directions, and the angle β between dipole moment and the ester group plane are listed in Table 4.

The MP2 method gives the largest value of the dipole moment (about 2.15 D). The dipoles computed at the B3LYP, B3PW91 and HF levels are in the range from 1.95 to 2.0 D, which corresponds better with the experimental values 1.79–1.97 D [35, 36, 37] (measured at room temperature in CCl_4 solution), but is probably still higher than in the gas phase. The solution values are usually higher than those measured in the gas phase. For example, for methyl acetate, the dipole moment measured in solution has values from 1.72 D to 1.83 D, [38, 39, 40]

Table 4 The values of the dipole moment μ, the angle α between the dipole and C=O bond directions, and the angle β between dipole moment and the ester group plane calculated for the HF. B3LYP, B3PW91 and MP2 theory levels

Basis set	Dipole moment μ(D)	Angle α (°)	Angle β (°)
HF			
6-31G**	2.016	4.7	0.1
B3LYP			
6-31G*	1.948	11.2	2.7
6-31G**	1.944	11.4	2.7
6-31+G*	2.007	10.3	1.7
6-31+G**	1.997	10.4	1.8
6-31++G*	2.008	10.4	1.8
6-31++G**	1.999	10.2	1.9
6-311++G**	1.940	10.2	1.5
B3PW91			
6-31G*	1.942	11.1	2.6
6-31G**	1.938	11.1	2.4
6-31+G*	1.996	10.5	1.7
6-31+G**	1.986	10.5	1.7
6-31++G*	1.995	10.5	1.8
6-31++G**	1.988	10.5	1.7
6-311++G**	1.929	10.3	1.4
MP2			
6-31G*	2.154	7.9	1.4
6-31+G*	2.169	10.3	0.2

whereas in the gas phase it is 1.67 D; [41] for ethyl acetate these values are 1.78–1.84 D in solutions [38, 42, 43, 44] and 1.78 D in the gas phase; [41] for ethyl benzoate they are 1.79–2.00 D [38, 45] and 1.95 D, [41] respectively.

In order to estimate the influence of intermolecular interaction on the phenyl benzoate dipole moment, calculations in the presence of solvent were performed. We have optimized the structure of the molecule using the PCM [46, 47] reaction field model at B3LYP/6-31+G*. For CCl_4 solvent (ε=2.228), the calculated dipole moment value was 2.277 D, with is about 13% higher then the value calculated for the isolated molecule.

The DFT predictions are more successful than those obtained from calculations by Körner et al. (2.65 D) [48] and determined by Adam and co-workers (2.45 D). [6]

The semiempirical methods PM3 and AM1 give dipole moment values of 1.9 D and 2.14 D, respectively. The PM3 result is very close to the experimental data, but the geometrical structure of the phenyl benzoate molecule predicted by this method is very poor, as mentioned above.

The direction of the dipole moment depends on the level of theory. The values of the α and β angles are connected with the relative position of the carboxyl group to the benzene ring (which is described by the dihedral angle φ_1). The dipole moment is almost parallel to the C=O bond direction ($\alpha \approx 5°$) and lies in the plane of the ester group ($\beta \approx 0°$) for $\varphi_1 \approx 90°$ (calculated at HF/6-31G** level). In the DFT calculations, the α angle change to about 10° ($\beta \approx 1.8°$) for the basis set with diffuse functions while $\varphi_1 \approx 65°$ and increase to 11° ($\beta \approx 2.5°$) for smaller basis sets without diffuse functions (the angle φ_1 ranged to 50°).

IR and Raman spectra

Experimental IR spectra of phenyl benzoate (in the solid and vapor phases, and its dilute solution in carbon tetrachloride) and Raman spectra (of the solid and liquid phase) are shown in Fig. 4. The frequencies and relative intensities of the bands measured in these spectra are summarized in Table 5. The available experimental matrix isolation data for the strongest bands are also shown. [49] Table 6 shows theoretical harmonic frequencies, absolute and relative IR and Raman intensities (with respect to the strongest band) together with the proposed assignments. For approximate characterization of the vibrations, we use the total energy distribution (M matrix) technique (TED). [23, 50] The last column in the table contains a qualitative mode decomposition for contributions higher than 10%. For the B3LYP/6-31G* calculational level, the mode decompositions are qualitatively similar and the assignments of the Table 6 apply quite well.

The calculated data originate from the scaled quantum mechanical force field (SQM) applied for the B3LYP/6-31+G* model. New scaling factors have been proposed for the stretching vibration of the ester group and they are listed in Table 7. The use of these factors results in a 6.4-cm^{-1} RMS difference between the observed and calculated frequencies (for bands below 1,800 cm^{-1}) in comparison to 9.8 cm^{-1} RMS for Pulay's original scaling-factor set. [24] The ν(CH) vibration range (3,000–3,200 cm^{-1}) has been excluded from the statistics because of the very strong anharmonic nature of the CH stretching vibrations, the overlapping of the bands, the presence of combination bands and the fact that these vibrations are strongly perturbed by Fermi resonance effects.

In Pulay's set the C–C, C–O and C=O stretching vibrations are scaled by the same scaling factor 0.922. For phenyl benzoate this leads to significant differences between the experimental and theoretical frequencies for the C–O and C=O bands (e.g. for ν(C=O) vibration: 1,723 cm^{-1} for Pulay's set, 1,760 cm^{-1} for our set, in comparison to 1,760 cm^{-1} for the experimental vapor phase data).

It should be mentioned that the proposed scaling factors are adequate for the phenyl benzoate molecule. A proper improvement of Pulay's scaling factors requires calculations on a wide set of molecules with the ester group.

To compare the theoretical and experimental results more easily, we have constructed theoretical spectra using the data in Table 6. In order to introduce broadening into the theoretical spectra we have used a full width at half-maximum (FWHM) of 10 cm^{-1} for the IR and of 5 cm^{-1} for the Raman spectra. This is consistent with the broadest

Table 5 Experimental frequencies, normalized IR absorbance and Raman intensities of phenyl benzoate

No.	Experimental IR[a]			Experimental Raman[a]	
	KBr palette	Solution in CCl_4	Vapour (Ar matrix)[b]	Solid state	Liquid (345 K)
1	–	–	–	–	–
2	–	–	–	–	–
3	–	–	–	–	66.0 (1)
4	–	–	–	~71 (<1)	–
5	–	–	–	164.3 (6)	171.5 (15)
6	–	–	–	186.5 (2)	
7	–	–	–	259.8 (3)	257.7 (7)
8	–	–	–	308.8 (2)	306.7 (2)
9	390.0 (2)	–	–	~388 (<1)	–
10	–	–	–	–	–
11	~412 (<1)	–	–	–	~411 (<1)
12	442.0 (2)	–	–	~440 (<1)	~439 (<1)
13	452.5 (4)	–	–	~451 (<1)	~454 (<1)
14	505.8 (13)	–	–	503.4 (1)	503.7 (2)
15	575.3 (5)	574.4 (5)	571.0 (3)	572.8 (1)	572.8 (3)
16	611.9 (2)	~611 (<1)	–	615.3 (4)	612.7 (6)
17	616.7 (2)	~616 (<1)			615.7 (6)
18	678.9 (9)	–	–	–	–
19	682.3 (9)	–	–	677.2 (6)	677.7 (4)
20	692.4 (35) 696.8 (42)	690.0 (25)	683.0 (11)	691.0 (3)	690.2 (2)
21	704.5 (71)	705.5 (84)	704.2 (17)	702.7 (2)	–
22	752.2 (51)	–	742.8 (9)	748.9 (4)	746.1 (5)
23	795.6 (1)	–	–	~798 (<1)	798.0 (1)
24	816.8 (5)	–	816.2 (2)	815.7 (4)	813.2 (4)
25	–	–	–	–	–
26	845.8 (3)	–	847.1 (9)	845.6 (6)	851.2 (9)
27	853.5 (5)	–	–	855.2 (7)	
28	916.2 (8)	912.8 (5)	912.7 (2)	922.7 (2)	913.5 (2)
29	922.0 (7)	~934 (<1)	949.4 (1)	~932 (<1)	~936 (<1)
30	933.5 (5)	948.0 (1)			
31	977.9 (1)	–	–	987.7 (3)	988.6 (2)
32	986.1 (2)	–	–	–	–
33	1,001.1 (18)	1,000.6 (4)	1,005.4 (5)	1,003.0 (100)	1,001.7 (100)
34					
35	–	–	–	–	–
36	1,025.6 (26)	1,026.1 (32)	1,024.7 (18)	1,026.6 (16)	1,024.5 (14)
37			[1,022]		
38	1,063.7 (65)	1,063.3 (52)	1,059.4 (40) [1,060]	1,063.3 (2)	1,062.7 (1)
39	1,070.5 (1)	–	–	–	–
40	1,080.6 (40)	1,080.1 (30)	1,074.9 (24) [1,079]	1,080.2 (2)	1,081.0 (1)
41	1,153.4 (16)	–	–	1,154.4 (4)	~1,156 (<1)
42	1,158.7 (10)			1,161.6 (5)	1,162.0 (11)
43	1,166.9 (22)	1,163.6 (22)	1,163.7 (17)	1,170.1 (10)	~1,172 (<1)
44	1,177.5 (21)	1,178.0 (25)	1,181.0 (27) [1,177, 1,163]	1,179.6 (18)	1,178.3 (7)
45	1,203.1 (78)	1,198.8 (100)	1,200.3 (100) [1,206]	1,193.5 (17)	1,197.0 (19)
46	1,264.3 (70)	1,263.8 (80)	1,260.2 (80) [1,266]	1,263.8 (13)	1,265.0 (17)
47	1,297.6 (4)	1,295.7 (2)	1,312.3 (5)	~1,297 (<1)	1,295.8 (1)
48	1,310.6 (6)	1,315.0 (5)		1,315.1 (3) ~1,328 (<1)	1,314.8 (2)
49	1,314.5 (6)				
50	1,328.5 (2)				
51	1,450.5 (26)	1,452.4 (15)	1,451.2(3)	1,452.4 (3)	1,452.0 (2)
52	1,456.7 (15)	1,457.2 (4)	1,456.6 (2)		
53	1,486.2 (25)	1,482.0 (9)	1,495.7 (21)	1,489.0 (1)	1,490.6 (1)
54	1,491.4 (14)	1,495.4 (24)	[1,499]	1,493.1 (1)	
55	1,585.0 (6)	1,586.4 (3)	–	1,588.7 (9)	1,589.0 (9)
56					
57	1,591.0 (20)	1,593.7 (8)	1,596.1 (11)	1,597.9 (23)	1,598.9 (30)
58	1,596.6 (20)	1,600.9 (6)	[1,598]		
59	1,729.7 (100)	1,744.6 (65)	1,760.2 (45)[1,756]	1,724.2 (31,)	1,738.9 (22)
60	3,019.0 (1)	–	3,053.7 (5)	3,058.9 (12)	3,060.0 (10)
61	3,042.8 (3)		3,082.6 (10)	3,066.5 (42)	3,071.8 (61)

Table 5 (continued)

No.	Experimental IR[a]			Experimental Raman[a]	
	KBr palette	Solution in CCl_4	Vapour (Ar matrix)[b]	Solid state	Liquid (345 K)
62	3,034.2 (2)			3,072.1 (78)	
63	3,057.4 (5)				
64	3,064.5 (3)				
65	3,071.3 (2)				
66					
67					
68					
69					

[a] IR absorbance and Raman intensities in brackets are normalized to 100 for the strongest band
[b] Data from matrix isolation study [49]

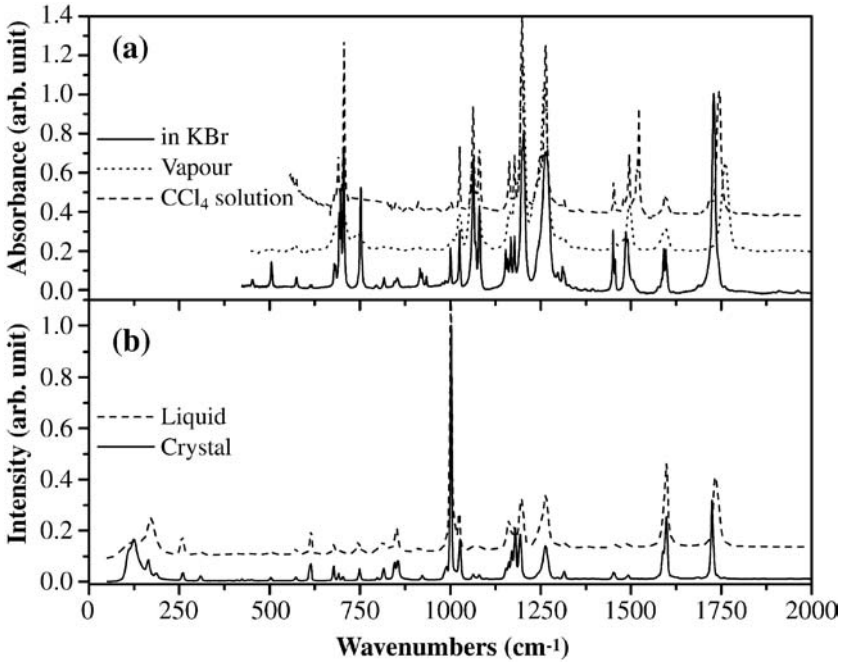

Fig. 4a–b Observed **a** IR and **b** Raman spectra of phenyl benzoate

bands in the experiment. As shown in Fig. 5, the calculated IR and Raman spectra agree almost perfectly with the experimental ones.

The calculated IR intensities reproduce the observed vapor spectrum very well, with the strong peaks corresponding to the stretching vibrations: C=O vibration (ν(C=O), 1,760 cm^{-1}), the symmetric C*–O (ν(C*–O), 1,260 cm^{-1}) and C–O (ν(C–O), 1,200 cm^{-1}) vibrations. A slight difference between calculated and experimental relative intensities results from the fact that the derivatives of the molecular dipole moments (which determine the calculated IR intensities) were obtained for the isolated molecule. For example, in the experimental vapor and CCl_4-solution spectra the ν(C–O) band is the strongest, while for the calculated spectrum the band ν(C*–O) has the highest intensity.

The most apparent differences are observed between the calculated spectrum and the experimental solid one. Especially evident is the shift of the ν(C=O) band; a change from 1,760 cm^{-1} for the vapor phase, to 1,744 cm^{-1} in the solution and to 1,730 cm^{-1} in the solid state. The intensity of the band varies in a meaningful way and becomes the highest for the IR spectrum of the solid. To estimate the influence of intermolecular interactions on the spectra, the PCM frequencies calculation has been performed for the B3LYP/6-31+G* theory level. For CCl_4 solution, the PCM reaction field model predicts the ν(C=O) peak at 1,791.0 cm^{-1} in comparison to 1,781.3 cm^{-1} for the isolated molecule (unscaled frequency). The calculated 9.7 cm^{-1} shift of the peak is in good agreement with the experimental results (15.6 cm^{-1}). The C=O stretching vibration appears to be the most sensitive to the transition from phase to phase.

The strongest bands at 1,260 and 1,200 cm^{-1} have been assigned to the ester group modes with participation of the ν_{13} C–H phenyl in-plane vibration (numbering of the phenyl ring vibration according to the Wilson's notation [51]). These vibrations lead to asymmetric C*–C, C*–O and C*–O, C–O bond-stretching, respectively. The symmetric C–O stretching vibration appears as a weak band at 847 cm^{-1} in the vapor phase.

Table 6 Calculated frequencies, IR and Raman intensities, and bands assignments of phenyl benzoate

No.	Calculated[a]			Assignment[b]
	Freq	IR	Raman	
1	20.9	0.3 (0)	396.3 (51)	τ(CO)
2	38.6	1.1 (0)	81.1 (10)	τ(C*O)+τ(CC*)
3	55.3	0.4 (0)	108.3 (14)	τ(CC*)+τ(C*O)
4	77.0	1.5 (0)	38.1 (5)	δ(COC*)+[δ(OC*C)]+[γ(OC)]+[τ(CO)]
5	163.6	0.2 (0)	94.2 (12)	γ(CC*)+τ(CC)
6	170.9	1.1 (0)	34.5 (4)	δ(CCC*)+δ(OC*C)+[τ(CC)]+[γ(CO)]
7	251.4	0.9 (0)	65.2 (8)	τ(CC)+[δ(COC*)]
8	307.9	6.9 (1)	36 (5)	ν(CC)+ν(C*C)
9	388.2	2.3 (0)	6.9 (1)	δ(CCC*)+[τ(CC)]+[δ(C=O)]
10	400.0	0 (0)	0.2 (0)	τ(CC) (16a)
11	405.7	0 (0)	17 (2)	
12	436.5	1.4 (0)	7.2 (1)	τ(CC)+[δ(CCC)] (16b)
13	455.1	1.3 (0)	5.2 (1)	τ(CC)+[γ(CC*)]+[δ(CCO)]
14	501.9	8.3 (2)	23.9 (3)	τ(CC)+γ(CO) (16b)
15	577.4	6.9 (1)	30.6 (4)	δ(CCC)+[δ(C=O)]+ [δ(OC*C)] (6a)
16	622.4	0.6 (0)	53 (7)	δ(CCC) (6b)
17	625.3	1 (0)	66.2 (8)	
18	667.0	2.4 (0)	0.8 (0)	δ(CCC)+[τ(CC)]+[δ(C=O)]
19	667.6	13 (3)	3.8 (0)	τ(CC) (4)
20	688.9	17.6 (4)	47.2 (6)	
21	708.8	87.5 (18)	2.2 (0)	γ(CH)+γ(C=O) (11)
22	746.9	51.9 (10)	69.9 (9)	γ(CH)+[γ(CO)] (11)
23	799.3	6.2 (1)	15.9 (2)	γ(C=O)+γ(CH)+γ(CC*)
24	817.3	7.4 (1)	73.6 (9)	ν(CC)+δ(CCC)+γ(CO)
25	830.9	1 (0)	16.8 (2)	γ(CH) (10a)
26	845.9	12.1 (2)	142.6 (18)	ν(OC*)+[δ(COC*)]+[δ(C=O)]+[γ(CH)]
27	856.2	0.1 (0)	3.2 (0)	γ(CH) (10a)
28	919.7	6.5 (1)	20.6 (3)	γ(CH)+[γ(CO)] (17b)
29	950.6	1.6 (0)	0.3 (0)	γ(CH) (17b)
30	964.2	0.2 (0)	1.7 (0)	γ(CH)+[τ(CC)] (17a)
31	988.0	0.1 (0)	0.1 (0)	γ(CH)+[τ(CC)] (17a)
32	988.9	1 (0)	37.3 (5)	γ(CH)+[τ(CC)] (5)
33	992.1	4.9 (1)	783.2 (100)	δ(CCC)+ν(CC) (12)
34	995.5	0.8 (0)	34 (4)	
35	1,006.7	0.1 (0)	0.9 (0)	γ(CH) (5)
36	1,016.2	18.5 (4)	1.7 (0)	ν(CC)+[δ(CCC)] (18a)
37	1,018.0	21.1 (4)	2.5 (0)	
38	1,056.3	146 (29)	42.4 (5)	ν(OC*)+[ν(CC)]+[δ(CH)]
39	1,065.8	10.5 (2)	3.2 (0)	
40	1,081.1	55.8 (11)	13.7 (2)	ν(CC)+δ(CH) (18b)
41	1,151.7	1.5 (0)	19.9 (3)	δ(CH)+ν(CC) (9b)
42	1,155.3	1.9 (0)	33 (4)	
43	1,158.4	21.8 (4)	45.5 (6)	δ(CH)+[ν(CC)] (9a)
44	1,168.0	56.6 (11)	56.3 (7)	
45	1,200.3	423.8(85)	451.4 (58)	ν(CO)+[ν(CC)]+[δ(CH)] (13)
46	1,260.0	499.4 (100)	629 (80)	ν(C*C)+ [ν(OC*)]+[δ(C=O)]
47	1,296.8	13.6 (3)	10.2 (1)	ν(CC)+δ(CH) (3)
48	1,307.4	10.5 (2)	15.1 (2)	
49	1,314.6	2.5 (1)	10.3 (1)	δ(CH)+ ν(CC) (14)
50	1,318.2	4.6 (1)	13.7 (2)	
51	1,443.3	16.8 (3)	23.4 (3)	δ(CH)+ ν(CC) (19b)
52	1,448.1	1.9 (0)	7.8 (1)	
53	1,482.7	47.5 (10)	13.4 (2)	δ(CH)+ν(CC) (19a)
54	1,487.6	16.2 (3)	12.8 (2)	
55	1,577.4	5 (1)	22.2 (3)	ν(CC)+[δ(CH)] (8b)
56	1,589.4	24.4 (5)	150.3 (19)	
57	1,592.8	19.2 (4)	161.9 (21)	ν(CC)+[δ(CH)] (8a)
58	1,598.2	9.5 (2)	440 (56)	
59	1,760.1	257.8 (52)	462.1 (59)	ν(C=O)
60	3,054.9	0.2 (0)	83.8 (11)	ν(CH)
61	3,055.6	0.3 (0)	66.3 (8)	
62	3,064.8	12.1 (2)	180.5 (23)	
63	3,066.2	14.6 (3)	176.1 (22)	
64	3,075.7	31.4 (6)	134.6 (17)	
65	3,075.9	21.5 (4)	277.3 (35)	
66	3,083.9	8.9 (2)	231.4 (30)	
67	3,091.6	6.2 (1)	134.3 (17)	
68	3,092.6	2.9 (1)	192.7 (25)	
69	3,099.2	3 (1)	145.6 (19)	

[a] Frequency (cm^{-1}), IR intensity (km mol^{-1}), Raman differential cross section(10^{-36} m^2/sr). IR absorbance and Raman intensities in brackets are normalized to 100 for the strongest band

[b] Contributions between 10% and 20% are given in square brackets. Wilson's symbols [51] for principal benzene bands are given in parentheses

Table 7 Scaling factors applied to the B3LYP/6-31+G* force field of phenyl benzoate

Description	Scaling factor
Stretching	
C=O	0.9632
O–C*	0.9486
C–C*	1.0046
C–O	0.9718
C–C	0.922[a]
C–H	0.920[a]
Bending	
C=O O–C*–C, C–O–C*, C–C–O and C–C–C*	0.990[a]
Phenyl ring	
C–H	0.950[a]
Out-of-plane	
C=O O–C and C–C* C–H	0.976[a]
Torsion	
Phenyl ring C–O, C*–O and C–C*	0.935[a]

[a] Fixed, from Pulay's set [24]

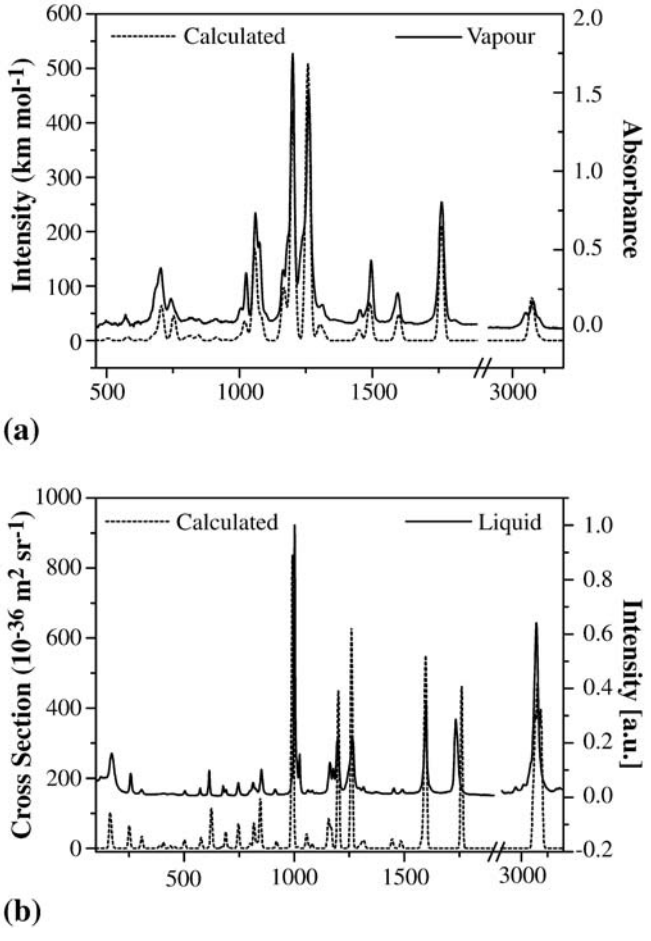

Fig. 5a–b Comparison of scaled (SQM B3LYP/6-31+G*) with experimental spectra of phenyl benzoate: **a** IR and **b** Raman spectra

In the range 1,600–1,300 cm^{-1}, aromatic compounds usually display five bands that are considered to be relatively pure C–C stretching vibrations. For phenyl benzoate, four peaks in the range 1,600–1,580 cm^{-1} have been assigned to the ν_{8a} and ν_{8b} vibrations. The ν_{8a} vibrations have been observed as medium intensity peaks at 1,598 cm^{-1} in the Raman and weak peaks in the IR spectra, whereas the ν_{8b} bands have very weak intensity and appear at 1,588 cm^{-1}. The ν_{19b} and ν_{19a} vibrations are weak but well separated and appear as two pairs of IR bands close to 1,490 and 1,450 cm^{-1}, respectively. The next C–C stretching modes, equivalent to the ν_{14} benzene vibration, were found around 1,315 cm^{-1} (two very weak lines).

Below 700 cm^{-1} the ring deformation modes are observed. The weak bands at 690 and 677 cm^{-1} were assigned to the C–C phenyl torsion vibrations, and those at 615 and 611 cm^{-1} to the ν_{6b} bending deformations. The very weak absorption around 574 cm^{-1} arises from the ν_{6a} bending deformation.

The C–H out-of-plane bending vibrations fall in the range from 1,000 to 700 cm^{-1}. Some of those bands are very weak: ν_5 (~989 cm^{-1}), ν_{17a} and ν_{17b} (in the range 960–910 cm^{-1}). Assignments in this region should be regarded as tentative. Only the ν_{11} modes near 750 and 702 cm^{-1} have medium intensity in the liquid and solid states.

Our band assignment is generally consistent with the results obtained from the HF/6-31G** calculations. [5] There are some differences for a few vibrations concerning the TED values obtained using the DFT and HF methods. These appear for the DFT modes 50, 49, 48, 47, 26, 25, 24 which correspond to the HF modes 48, 47, 50, 49, 25, 24 and 26, respectively.

Conclusions

The geometric parameters, conformational properties, dipole moment and the vibrational spectroscopic data of phenyl benzoate have been calculated at various levels of theory (HF, B3LYP, B3PW91 and MP2), using basis sets from 6-31G* to 6-311++G** (for the DFT methods).

For structural parameters, the best agreement between experiment and theory was obtained at the MP2, B3LYP and B3PW91 levels with those basis sets that include diffuse functions (the best results for the MP2/6-31+G* calculations). Therefore, it is necessary to use a basis set with diffuse functions in order to obtain correct dihedral angles of the ester group. Taking into account the time consumed for calculations at different theory levels, it seems that the B3LYP/6-31+G* level is the best choice for determining the structure of liquid crystal molecules.

The potential scans computed at the B3LYP/6-31+G* theory level gave a reasonable estimation of the phenyl ring torsion around the C(phenyl)–O(ester) and C(ester)–C(phenyl) bonds.

The dipole moment calculated at the DFT levels is only 10% higher than the experimental value measured in solution.

The SQM method was used for scaling the B3LYP/6-31+G* harmonic force field. The calculated IR and Raman spectra are in very good agreement with the vibrational experimental data. Reliable and almost complete assignments of the vibrational bands have been made.

Acknowledgement This work was partly supported by the Committee for Scientific Research (KBN) under Grant No. 2P03B09817. The authors thank Prof. P. Pulay for the SQM program and Dr. A. Jarzecki for help.

References

1. Bone MF, Price AH, Clark MG, McDonnel DG (1982) Liq Cryst Ordered Fluids 4:799–805
2. Wrzalik R, Merkel K, Kocot A, Ciepłak B (2002) J Chem Phys 117:4889–4895
3. Adams JM, Morsi SE (1976) Acta Crystalogr B32:1345–1347
4. Shibakami M, Sekiya A (1995) Acta Crystalogr C51:326-330
5. Tsuji T, Takeuchi H, Egawa T, Konaka S (2001) J Am Chem Soc 123:6381–6387
6. Adam CJ, Clark SJ, Ackland GJ, Crain J (1997) Phys Rev E 55:5641–5649
7. LeFevre RJ, Sudaram AJ (1962) J Chem Soc 3904–3915
8. Bogatyreva IK, Avakyan VG, Khodjaeva VL (1995) Izv Acad Nauk Ser Khim 3:443–447
9. Emsley JW, Furby MI, De Luca G (1996) Liq Cryst 21:877–883
10. Frisch MJ, Trucks GW, Schlegel HB, Scuseria GE, Robb MA, Cheeseman JR, Zakrzewski VG, Montgomery JA, Stratman RE, Burant JC, Dapprich S, Millam JM, Daniels AD, Kudin KN, Strain MC, Farkas O, Tomasi J, Barone V, Cossi M, Cammi R, Mennucci B, Pomelli C, Adamo C, Clifford S, Ochterski J, Petersson GA, Ayala PY, Cui Q, Morokuma K, Malick DK, Rabuck AD, Raghavachari K, Foresman JB, Cioslowski J, Ortiz JV, Baboul AG, Stefanov BB, Liu C, Liashenko A, Piskorz P, Komaromi, I, Gomperts R, Martin RL, Fox DJ, Keith T, Al-Laham MA, Peng CY, Nanayakkara A, Gonzalez C, Challacombe M, Gill PMW, Johnson BG, Chen W, Wong MW, Andres JL, Gonzales C, Head-Gordon M, Replogle ES, Pople JA (1998) Gaussian 98. Gaussian, Pittsburgh Pa.
11. Hehre WJ, Radom L, Schleyer PvR, Pople JA (1986) Ab initio molecular orbital theory, 1st edn. Wiley, New York, pp 20–29, 65–88
12. Frisch MJ, Head-Gordon M, Pople JA (1990) Chem Phys Lett 166:275–280
13. Hohenberg P, Kohn W (1964) Phys Rev B 136:864–871
14. Kohn W, Sham LJ (1965) Phys Rev A 140:1133–1138
15. Parr RG, Yang W (1989) Density functional theory of atoms and molecules, 1st edn. Oxford University Press, New York, pp 142–197
16. Becke AD (1993) J Chem Phys 98:5648–5652
17. Becke AD (1988) Phys Rev A 38:3098–3100
18. Lee C, Yang W, Parr RG (1988) Phys Rev B 37:785–789
19. Vosko SH, Wilk L, Nusair M (1980) Can J Phys 58:1200–1211
20. Perdew JP, Chevary JA, Vosko SH, Jackson KA, Pederson MR, Singh DJ, Fiolhais C (1992) Phys Rev B 46:6671–6687
21. Perdew JP, Burke K, Wang Y (1996) Phys Rev B 54:16533–16539
22. Pulay P, Fogarasi G, Pongor G, Boggs JE (1979) J Am Chem Soc 101:2550–2560
23. Pulay P, Fogarasi G, Pongor G, Boggs JE, Vargha A (1983) J Am Chem Soc 105:7037–7047
24. Rauhut G, Pulay P (1995) J Phys Chem 99:3093–3100
25. Kozłowski PM, Zgierski MZ, Pulay P (1995) Chem Phys Lett 247:379–385
26. Merkel K, Wrzalik R, Kocot A (2001) J Mol Struct 563–564:477–490
27. Kon M, Kurokawa H, Takeuchi H, Konaka SJ (1992) J Mol Struct 268:155–167
28. Kiyono H, Tatsunami R, Kurai T, Takeuchi H, Egawa T, Konaka S (1998) J Phys Chem 102:1405–1411
29. Sun H (1994) J Comput Chem 15:752–768
30. Radom L, Pople JA (1970) J Am Chem Soc 92:4786–4975
31. Ortí E, Sánchez-Marín J, Marchán M, Tomás F (1987) J Phys Chem 91:545–551
32. Meier RJ, Koglin E (2002) Chem Phys Lett 353:239–243
33. Kristyán S, Pulay P (1994) Chem Phys Lett 229:175–180
34. Kurita N, Sekino H (2001) Chem Phys Lett 348:139–146
35. Berdikhin AA, Frolova LV, Prangova LS, Vulfson SG (1992) J Gen Chem USSR 62:1921–1926
36. Irvine PA, Erman B, Flory PJ (1983) J Phys Chem 87:2929–2935
37. Prangova LS, Fradkina SP, Vasileva IN (1987) J Gen Chem USSR 57:1656–1667
38. Lide DR (2001) Handbook of chemistry and physics, 81st edn. CRC Press, New York, pp 9.44–9.50
39. Bredikhin AA, Kirillovich VA, Vereshchagin AN (1988) Bull Acad Sci USSR Div Chem Sci 37:678–682
40. Tarasova GV, Khashchina MV, Tyurin SA, Bulgarevich SB, Bogdan IG (1986) Russ J Phys Chem 60:1235–1238
41. Abboud JLM, Notario R (1999) Pure Appl Chem 7:645–718
42. Saxena SK, Shukla JP, Saxena MCh (1980) Bull Chem Soc Jpn 53:1731–1735
43. Bredikhin AA, Kirillovich VA (1988) Bull Acad Sci USSR Div Chem Sci 37:931–934
44. Kano Y, Minami R, Takahashi H (1980) Bull Chem Soc Jpn 53:642–644
45. Gumennyi VI (1987) Chem Heterocycl Compd 23:1288–1292
46. Miertus S, Scrocco E, Tomasi J (1981) J Chem Phys 55:117–129
47. Cammiv R, Tomasi J (1995) J Comput Chem 16:1449–1458
48. Körner H, Shiota A, Bunning TJ, Ober CK (1996) Science 272:252–255
49. Sander WW (1989) J Org Chem 54:333–339
50. Pulay P, Török F (1966) Acta Chem Acad Sci Hung 47:273–297
51. Wilson EB, Decius JC, Cross PC (1995) Molecular vibrations, 1st edn. McGraw-Hill, New York